A Multiple-Functional Ag/SiO_2/Organic Based Biomimetic Nanocomposite Membrane for High-Stability Protein Recognition and Cell Adhesion/Detachment

Yilin Wu, Ming Yan, Jiuyun Cui, Yongsheng Yan, and Chunxiang Li**

Biomimetic multilevel structured membrane materials have great potential for energy-efficient chemical separations and biomedical applications. The current study represents a simple, yet efficient, method to obtain the biomimetic protein separation membrane and controllable cell culture substrate with high stability, selectivity, and antibacterial property. Here, a molecular imprinting methodology is reported to introduce the high-biocompatible protein ovalbumin (Ova) to a multilevel Ag/SiO_2/organic based molecularly imprinted membranes (ASO-MIMs), which have made significant achievements in protein identification and controllable growth of liver cells in vitro platform. Interestingly, the relative morphological observations of the adhered cells and in vitro viability tests show no significant difference between the ASO-MIMs binding with 13.6 mg g^{-1} Ova (13.6-ASO-MIMs) and bare glass, indicating the excellent biocompatibility of the 13.6-ASO-MIMs. Here, the results on largely enhanced adsorption capacity, perm-selectivity (β values are more than 2.2), regeneration ability (still maintained 90% of the maximum adsorption capacity after 10 cycling operation), and high-performance cell adhesion system (controlled by the binding amount of template protein) are shown, which clearly demonstrates the potential value of this method in smart biomaterials and biosensors.

1. Introduction

Development of multiple-functional porous membranes capable of recognizing and separating specific objects with high stability, antibacterium, and most recently biocompatibility are of considerable interest in biomimetic multilevel structured nanomaterial (BMSN) and cell-based adhesion technology.[1–7] Recent studies have shown that introduction of cell-adhesive biomolecules to the BMSN or cell culture surfaces can largely improve their biocompatibility which holds great promise in biomedical engineering applications.[8–10] More recently, molecular imprinting technology (MIT) is regarded as an attractive mimetic approach to create specific recognition cavities chemically complementary and geometrically to target molecule with nonbiological strategy.[11–14] It is also well-known that, molecularly imprinted membranes (MIMs) are the membranes composed of molecularly imprinted polymers (MIPs) or containing MIPs. Therefore, combination of MIPs into nanoporous membranes can provide membrane-based specific separation for target molecules.[15] Although some studies have proven that the molecular imprinting of proteins could be obtained through the optimization of MIT, the achievement of protein imprinting membrane materials with excellent perm-selectivity, chemical stability, biocompatibility, and regeneration ability is still facing challenges.[16–18]

It goes without saying that an ideal imprinted membrane should have high permeability, chemical stability, and antibacterial property simultaneously. Recently, increase in awareness and understanding of these factors have governed many active works such as physical blending, chemical grafting, and surface modification to improve the comprehensive performance of various polymer membranes.[19–21] Despite decades of tremendous progress in this field, issues such as protein separation, low regenerability, poor chemical selectivity, and reduced structure resistance still exist.[22] Regarding to these aspects, nanosized particles have been smartly utilized for modification of membranes to meet different requirements. To date, applications of such nanocomposite membranes have made great progress in such fields as water purification, drug delivery, biomolecule separation, electronic industries, dairy, and food.[23–25] However, many inherent drawbacks such as weak binding force, nonuniform dispersion, and loosely binding of inorganic nanoparticles on the membrane surfaces have proven to be extremely challenging to obtain the high-performance separation membranes.

Consequently, finding new avenue to manipulate the surface chemistry and the nature of functionality of intrinsic layered structural membranes is of paramount importance to gain the novel protein-imprinted BMSN with high-stability, multifunctionality, and regeneration properties. Inspired by mussel-adhesion phenomena in nature, dopamine is discovered as a promising bioinspired material for membrane

Dr. Y. L. Wu, J. Y. Cui, Prof. Y. S. Yan, Prof. C. X. Li
College of Chemistry and Chemical Engineering
Jiangsu University
Zhenjiang 212013, China
E-mail: yanyongsheng321123@163.com;
w526249292@163.com
Dr. M. Yan
College of Material Science and Engineering
Jiangsu University
Zhenjiang 212013, China

DOI: 10.1002/adfm.201502465

© 2015 WILEY-VCH Verlag GmbH & Co. KGaA, Weinheim

modifications.[26,27] Recently, the surface formative hydrophilic polydopamine (pDA) structure is an extremely versatile platform for integrating nanoparticles (TiO_2/SiO_2/Ag/Au etc.) within versatile materials, called polydopamine-assisted inorganic film formation (pIFF, Figure S1, Supporting Information).[28–30] Compared with some commonly used stabilization materials, this technique allows for the large improvement of durability, mechanical strength, and antifouling performance because it synergizes the chemical stability and mechanical strength of porous membranes with the uniform dispersion and tightly binding of modified nanoparticles on membrane surfaces.[31–33]

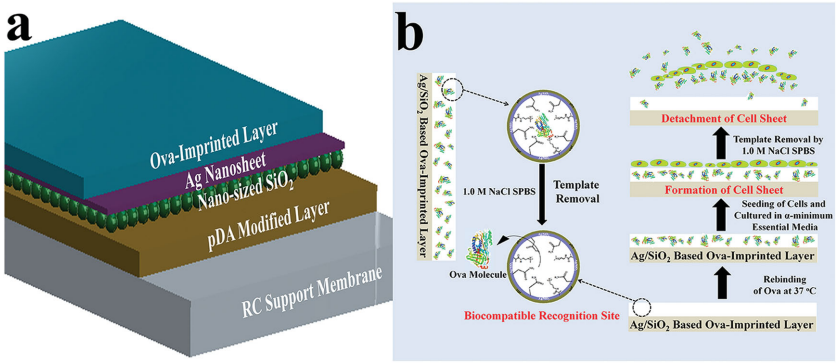

Scheme 1. a) Schematic view of the Ag/SiO_2/organic based Ova-imprinted membrane structure. b) Schematic illustration for the template protein recognition and cell sheet formation and detachment.

To address the above-mentioned issues, we herein report a multilevel Ag/SiO_2/organic based nanoporous composite technique and device for harvesting protein-imprinted membranes and cell culture substrate with controllable biocompatibility. For the first time, a simple two-step functionalization approach was developed on the pDA modified surfaces to obtain the uniformly bound SiO_2/Ag nanosheet structure. The imprinting process was then performed by optimized redox-initiated polymerization to prepare the Ag/SiO_2/organic hybrid MIMs (ASO-MIMs). In this case, ovalbumin (Ova, pI 4.6), the high-biocompatible scaffold from hen egg white (HEW), was chosen as the template bioprotein to demonstrate the proof-of-principle of our strategy.[9,10,18] In contrast to the introduction of bioprotein by means of physical absorption and covalent binding, the synthesized hybrid structure cannot only largely enhance the permselectivity and regenerability of membrane, but also significantly promotes cell adhesion/detachment during cell culture. To the best of our knowledge, this is the first demonstration of the Ag/SiO_2/pDA-based surface as a support to biofunctionalize MIMs for the formation of biomimetic multilevel structure. In addition, because of the high affinity of the as-prepared ASO-MIMs (comparable to that of the natural receptor) and the innocuity to bioprotein (compared to covalent interactions), the approach reported here can be seen as a promising candidate for large-scale application in specific protein recognition, separation, and cell-based regenerative medicine.

2. Results and Discussion

The key design of our synthetic methodology was to incorporate the specific cell adhesion sites (protein-imprinted sites) and cell growth substrate into the Ag/SiO_2/organic based porous hybrid MIMs (ASO-MIMs, **Scheme 1**a). In this work, a bio-inspired "self-assembly composite" technique was explored to introduce the versatile secondary reaction platform (the pDA-based surface). The synthesis pathway of the ASO-MIMs involved two main steps. Initially, a two-step functionalization approach was developed on a mussel-inspired porous surface to obtain the uniformly bound SiO_2/Ag nanosheet structure. Second, to achieve the best affinity between target bioprotein and the ASO-MIMs during cell culture, the imprinting process was performed by redox-initiated polymerization at 37 °C in sterile phosphate-buffered saline (SPBS) using Ova as the template bioprotein (Figure S2, Supporting Information). Following that, the Ova templates were removed by washing with SPBS containing 1.0 M NaCl (1.0 M NaCl SPBS). This ultimately achieved coupling of biocompatible cell growth environment with its underlying extracellular matrix (ECM) onto the surfaces of ASO-MIMs by adsorbing and eluting Ova molecules (Scheme 1b).

To demonstrate the wide applicability of our method, the morphological evolution of various synthesized membranes was examined by field emission scanning electron microscopy (SEM). As shown in **Figure 1**a, the pristine regenerated cellulose membrane (RC) exhibited a typically porous structure with a fairly smooth surface. Figure 1b showed the SEM images of the pDA modified RC (pDA@RC) fully covered with pDA layers at low and high magnifications. Meanwhile, the pristine RC turned from white to dark brown during the dopamine medication process (Figure S3, Supporting Information). The attenuated total reflection-Fourier transform infrared spectroscopy (ATR-FTIR) characterization was also investigated to confirm the formation of pDA films on RC surfaces (Figure 1c). Compared with pristine RC, pDA@RC displayed several new absorption peaks at 1506 and 1620 cm^{-1}, which suggested the occurrence of N—H bending vibrations and C=C resonance vibrations, respectively. In addition, a new broad absorbance between 3500 and 3000 cm^{-1} was ascribed to O–H and NH_2 stretching vibrations.[34,35] In Figure 1d, SiO_2 layer composing of plentiful SiO_2 nanoparticles can be observed on the top surfaces of pDA@RC (SiO_2@pDA@RC). Meanwhile, the energy-dispersive X-ray spectroscopy (EDX, Figure S4a, Supporting Information) also indicated that the sample was composed of Si, N, C, and O. After the acid-directed Ag assembly process on SiO_2@pDA@RC surface (Figure 1e), a typically sheet-like Ag nanosheet structure could be obtained whilst new Ag element emerged in the EDX spectrum (Figure S4b, Supporting Information), indicating the formation of Ag nanosheets on the membrane surface (Ag-SiO_2@pDA@RC). When comparing Ag-SiO_2@pDA@RC (Figure 1e) and 3-methacryloxypropyltrimethoxysilane (MPTS) modified Ag-SiO_2@pDA@RC (Figure S5a, Supporting Information, MPTS-Ag-SiO_2@pDA@RC), the physical difference observed in the SEM images was

© 2015 WILEY-VCH Verlag GmbH & Co. KGaA, Weinheim

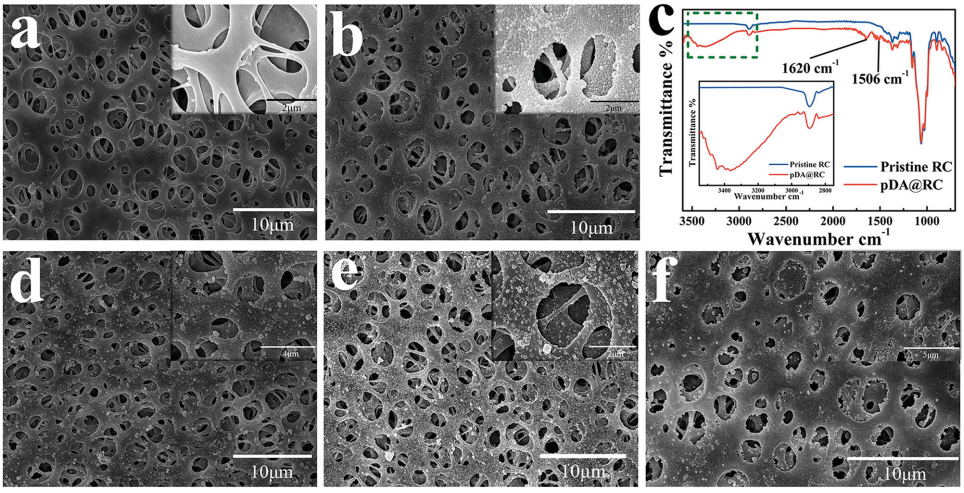

Figure 1. Surface characterizations of different synthesized membranes. Overview SEM images of a) pristine RC membrane, b) pDA@RC, d) SiO_2@pDA@RC e) Ag-SiO_2@pDA@RC, f) ASO-MIMs with different magnifications. c) ATR-FTIR spectra of pristine RC and pDA@RC (inset is magnifying spectra from 2800 to 3600 cm^{-1}).

very slight because the MPTS grafts were amorphous molecule layers. Nonetheless, the modification of MPTS on the Ag-SiO_2@pDA@RC was also confirmed by ATR-FTIR (Figure S5b, Supporting Information), a new signal at 1690 cm^{-1} was obtained that is assigned to CH_2=CH_2 stretching modes, which clearly demonstrated the formation of MPTS layers.[36] Compared with other modified membranes, the obvious polymer layers could be obtained on the ASO-MIMs surface, strongly indicating the readily coating of Ova-based imprinted layers after the redox-initiated polymerization (Figure 1f). To further study the element distribution of our ASO-MIMs, the elemental mapping by EDX analysis was used render a detectable signal-to-noise ratio (Figure S6, Supporting Information). Assisted by the mapping technique, the distributions of Ag, Si, N, and C elements strongly proved the homodisperse and uniform location of synthesized multiple-functional structure.

Furthermore, X-ray photoelectron spectroscopy (XPS) wide scans (**Figure 2**a) and narrow scans (Figure 2b–e) were studied to further analyze the surface composition of various synthesized membranes. Compared with the pristine RC, the full XPS spectrum survey of pDA@RC given in Figure 2a showed the presence of N, together with the narrow scan for C1s peaks of pDA@RC (Figure 2b), demonstratively indicating the formation of pDA layers.[31] After SiO_2 modification of the pDA@RC, the new emerging Si2s and Si2p peaks, together with the XPS-peak-differenating analysis (Figure 2c) clearly demonstrated

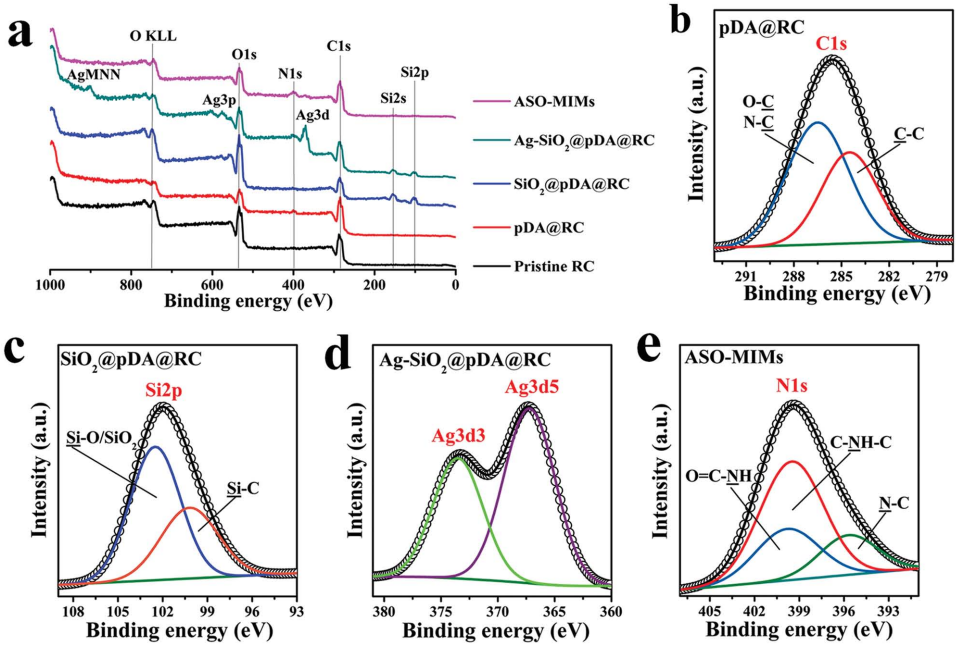

Figure 2. a) XPS wide scans of various synthesized membranes and narrow scans for b) C1s, c) Si2p, d) Ag3d, and e) N1s peaks.

© 2015 WILEY-VCH Verlag GmbH & Co. KGaA, Weinheim

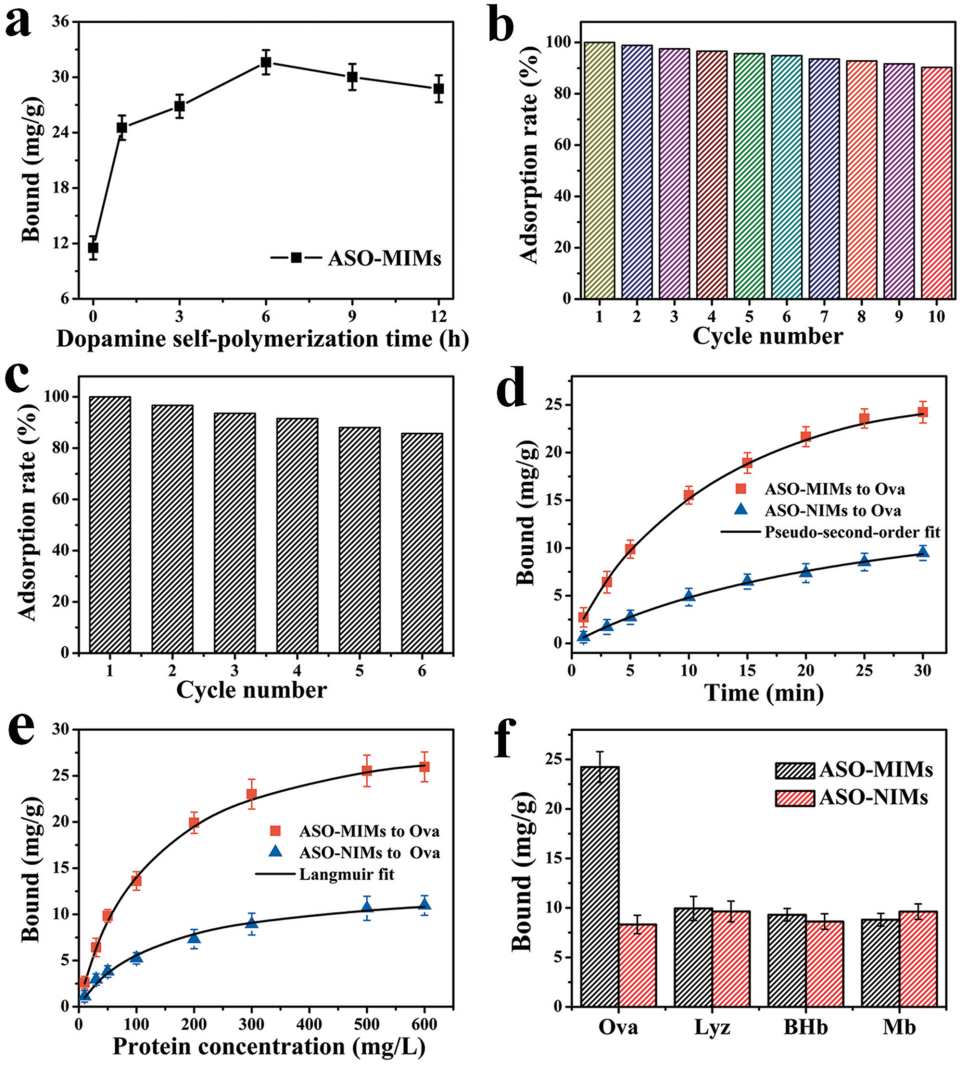

Figure 3. a) Effect of the dopamine self-polymerization time on the recognition behavior of the ASO-MIMs toward Ova. Cycling operations and regeneration performance of b) ASO-MIMs and c) ASO-MIMs-0. d) Kinetic data and modeling for the adsorption of Ova molecules onto ASO-MIMs and ASO-NIMs. e) Adsorption isotherms at 37 °C of Ova (ranging from 10 to 600 mg L^{-1}) on ASO-MIMs and control ASO-NIMs with the fitting to Langmuir model. f) Binding amounts of different proteins on ASO-MIMs and ASO-NIMs. The Ova amount was determined by using HPLC analysis. The points represent mean values of three measurements.

the presence of assembled SiO_2 structures. Similarly, the new emerging Ag3d and Ag3p peaks could be observed in the Ag-SiO_2@pDA@RC, suggesting the formation of the Ag nanostructure (Figure 2d). Finally, as shown in Figure 2a, the Ag3d and Ag3p peaks of ASO-MIMs were almost shielded. Instead, the intensity of N1s and O1s peaks enhances, and the binding peaks of O=C–NH and C–NH–C emerged (which were ascribed to the polymerization monomers), indicating the formation of the imprinted layers on membrane surfaces (Figure 2e). In addition, the XPS curve-fitting results of O1s were also studied in detail to further prove the appearance of the new electronic structures. The O1s peak of pDA@RC with two typical peaks (C–OH and C=O) are corresponding to the groups in pure pDA (Figure S7a, Supporting Information).[31] As shown in Figure S7b, Supporting Information, the new curve of SiO_2/Si-O could be obtained, suggesting the successful conduction of the hydrolysis process of tetraethyl orthosilicate (TEOS) on the pDA@RC surface. For Figure S7c, Supporting Information, after the redox-initiated polymerization process, only three curves of C–OH, O–C–O, and C=O could be obtained, demonstrating the complete coating of imprinting layers in presence of the methylene bisacrylamide (MBAA) and acrylamide (AAm).

As is well-know, the comprehensive performance of binding capacity, stability, and durability of a molecularly imprinted material is all-important for its large-scale applications.[11,12] In this work, to obtain efficient protein recognition, the synthesis conditions of Ova-imprinted ASO-MIMs were all investigated in detail and the rebinding capacities of ASO-MIMs toward target protein were optimized (**Figure 3**a and Figure S8, Supporting Information). Figure 3a described the relationship of the dopamine self-polymerization time to the binding capacity

© 2015 WILEY-VCH Verlag GmbH & Co. KGaA, Weinheim

of the synthesized ASO-MIMs. As shown, the binding capacity increased linearly as the dopamine self-polymerization time increasing from 0 to 6 h. On the contrary, when the polymerization time was above 6 h, an obvious reduction in the adsorption capacity of ASO-MIMs could be observed. Importantly and interestingly in this case, when the ASO-MIMs were synthesized without the surface functionalization of dopamine (ASO-MIMs-0, dopamine self-polymerization time is 0 h), a much smaller binding capacity than that of other membranes was obtained (less than one half of the optimized value). In addition, the effect of the dopamine self-polymerization time on the adsorption capacities of nonimprinted membranes (ASO-NIMs) was also studied. In comparison with ASO-MIMs (Figure 3a), the binding capacities of ASO-NIMs increased slightly and linearly as the dopamine self-polymerization time increasing (Figure S9, Supporting Information), which strongly suggested the significant effects of pDA-based layers for the fabrication of imprinting sites in our ASO-MIMs, as reported in Figure 3a and our previous work.[37] More importantly, the stability and regeneration comparison between the ASO-MIMs and ASO-MIMs-0 were studied by developing a cycling operation (adsorption/desorption process). As shown in Figure 3b, through the formation of strong covalent chemical bounds, the rebinding capacity of the ASO-MIMs sample was not obviously lost after 10 recycles and the adsorption rate is still higher than 90% of the maximum adsorption capacity during the 10th and last cycle. As the control, the ASO-MIMs-0 was also used for determining its regeneration performance, the ASO-MIMs-0 sample only left 85% rate of the maximum adsorption capacity of ASO-MIMs-0 after just six recycles (Figure 3c), which strongly illustrated the excellent durability, and regeneration ability of our mussel-inspired synthetic methodology.

To further confirm the recognition ability of ASO-MIMs, the static adsorption experiments were carried out by batch mode operations. The adsorption kinetics experiments were proceeded using 500 mg L^{-1} Ova SPBS to investigate the rate-controlling and binding mechanism of the as-prepared ASO-MIMs and ASO-NIMs. The kinetic curves shown in Figure 3d and data in Table S1, Supporting Information, demonstrated a remarkable rapid adsorption dynamics of Ova protein to ASO-MIMs than that of ASO-NIMs and other MIMs reported previously (the Ova-imprinted ASO-MIMs took up nearly 85% of the equilibrium amount of the templates within a period of 15 min).[38–41] That is to say, a great number of effectively imprinting sites were created on the ASO-MIMs surfaces during the imprinting process. To further study the rate-controlling mechanism, the pseudo-first-order rate equation[42] and pseudo-second-order rate equation[43] were applied to further analyze the kinetic data (see Table S1, Supporting Information). The binding isotherms of Ova molecules onto ASO-MIMs and ASO-NIMs at 37 °C were shown in Figure 3e. It is observed that the ASO-MIMs possessed a much higher binding capacity of Ova than that of ASO-NIMs at any adsorption concentrations, which directed the successful conduction of redox-initiated polymerization on the surface of Ag-SiO_2@pDA@RC. Langmuir model[44] was also applied and fitted well with the obtained rebinding data (see Table S2, Supporting Information).

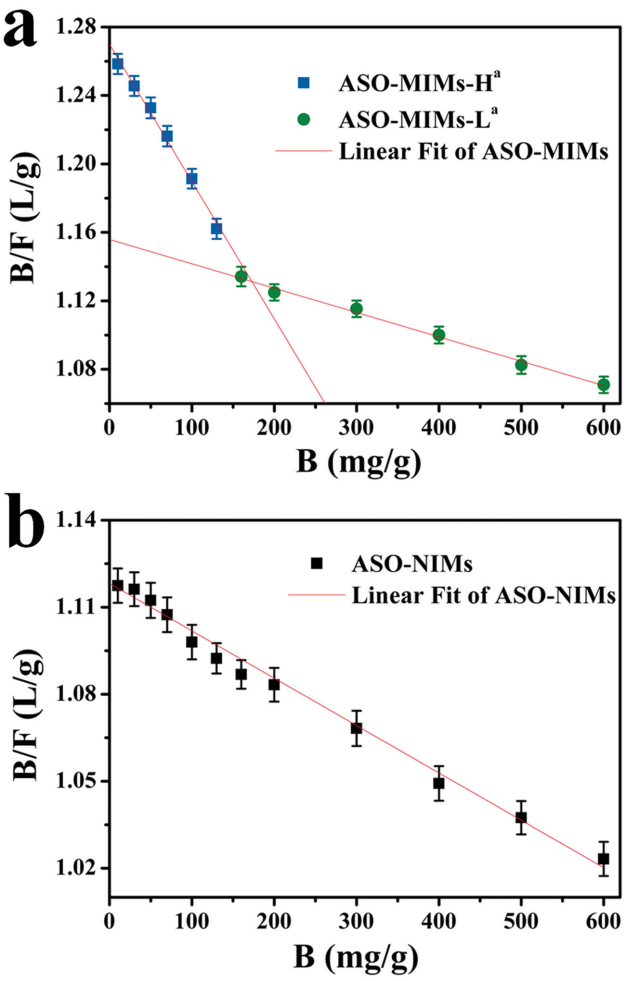

Figure 4. Scatchard plots of the a) ASO-MIMs and b) ASO-NIMs. [a]ASO-MIMs-H and ASO-MIMs-L refer to the high-affinity sites (specific recognition sites) and low-affinity sites (nonspecific recognition sites), respectively.

To prove recognition specificity of our ASO-MIMs, lysozyme (Lyz, pI 10.8), bovine hemoglobin (BHb, pI 7.0), and myoglobin (Mb, pI 7.1) were chosen for comparison, which have large differences in molecular structure and dimension with Ova. The ASO-MIMs showed a very sensitive response to the original template Ova but were almost insensitive to nontemplate proteins (Lyz, BHb, Mb) (Figure 3f), suggesting the creation of plenty of specific recognition sites for templates in ASO-MIMs. Meanwhile, the scatchard plots shown in **Figure 4** and data in **Table 1** demonstrated that there existed two distinct populations of binding sites in the ASO-MIMs: high affinity sites (i.e., "specific recognition sites") and low affinity sites (i.e., nonspecific recognition sites). The results indicated that, besides "specific recognition sites" for Ova which were formed during imprinting process, nonspecific binding sites also existed. And it also clearly indicated that a large number of binding sites with a markedly higher association constant were presented in the ASO-MIMs (Figure 4a), but not in the ASO-NIMs (Figure 4b).

Transport studies of MIMs could provide an incisive comprehension about the relationship between the arrangements

© 2015 WILEY-VCH Verlag GmbH & Co. KGaA, Weinheim

Table 1. The isothermal binding parameters determined from Scatchard plots.

Sample	K_a [$\times 10^4$ M^{-1}]	N_{max} [mg g^{-1}]	$R^{2a)}$
ASO-MIMs-H	7.99	15.89	0.9945
ASO-MIMs-L	2.63	39.75	0.9951
ASO-NIMs	1.99	55.91	0.9946

[a)]Correlation coefficient of fitting.

Table 2. Time-permeation results (after 60 min) of ASO-MIMs and ASO-NIMs for Ova, Lyz, BHb, and Mb. The data are the mean of at least three independent experiments.

Membranes	Substrates	J [mg cm^{-2} h^{-1}]	P [cm^2 h^{-1}]	$\beta_{Lyz/Ova}$	$\beta_{BHb/Ova}$	$\beta_{Mb/Ova}$
ASO-MIMs	Ova	5.21	2.21	2.55	2.49	2.25
	Lyz	8.11	5.63			
	BHb	8.04	5.51			
	Mb	7.73	4.97			
ASO-NIMs	Ova	8.65	6.83	0.90	1.04	0.98
	Lyz	8.36	6.14			
	BHb	8.77	7.13			
	Mb	8.61	6.72			

of functional groups and the shape of the recognition sites in imprinting cavities. During the redox-initiated imprinting process on membrane surfaces, the specific recognition cavities predetermined by shape and size of Ova molecules were obtained after the removal of templates in the fixation of the linking groups. To further confirm the specific recognition mechanism and separation performance of our ASO-MIMs toward target protein, time-dependent permeation operations and static transport experiments were carried out to study and evaluate the imprinting effects of the as-prepared ASO-MIMs. As shown in Figure S10, Supporting Information, the permeation tests were performed by an H-model tube installation. As shown in **Figure 5**a,b, time-dependent perm-selectivity experiments were performed using Ova, BHb, Lyz, and Mb as competitive transport proteins, and the permeability coefficients are summarized in **Table 2**. The ASO-MIMs exhibited lower transport rates and permeation flux of Ova molecules than that of other analogues, which should be mainly attributed to the presence of sterically complementary imprinting cavities of templates (Ova) that hindered the transport of template protein via binding/desorption onto the nanosized Ag@SiO_2-based imprinting sites on ASO-MIMs surfaces. In contrast, when comparing Figure 5a with Figure 5b, a contrary permeation performance could be observed in ASO-NIMs. The ASO-NIMs exhibited nearly the same transport performance of Ova, BHb, Lyz, and Mb proteins, it should be mainly because that the nonformation of imprinting cavities in ASO-NIMs, so nonimprinting effects could be achieved by ASO-NIMs in the permeation experiments. Therefore, the random arrangement of the functional groups of monomers in ASO-NIMs resulted in no imprinting and selective separation effects.

In order to obtain a deeper understanding about the perm-selectivity isomers of the as-prepared ASO-MIMs, the static permeation performance of the ASO-MIMs and ASO-NIMs toward templates with different initial permeation concentrations (ranging from 50 to 600 mg L^{-1}) was studied to confirm

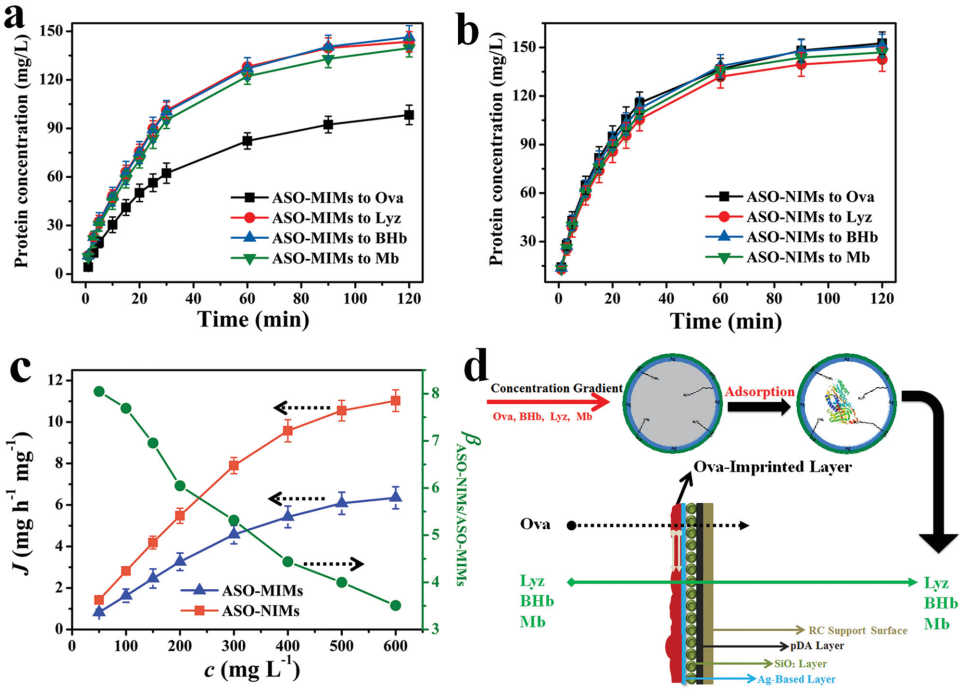

Figure 5. Time-dependent perm-selectivity curves of Ova, BHb, Lyz, and Mb through a) ASO-MIMs and b) ASO-NIMs. c) Static transport performance of ASO-MIMs and ASO-NIMs toward Ova. d) Schematic representation of the selective permeation performance of ASO-MIMs.

© 2015 WILEY-VCH Verlag GmbH & Co. KGaA, Weinheim

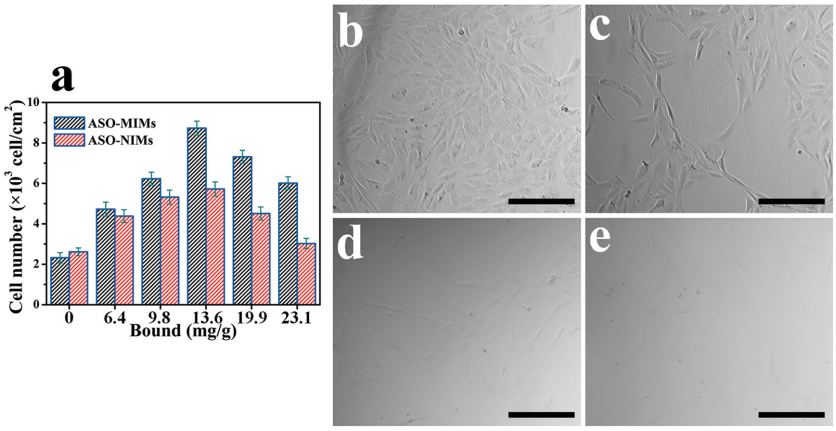

Figure 6. a) Effect of the amount of bound Ova on cell adhesion for both the ASO-MIMs and ASO-NIMs after 2 h of culture. The Ova amount was determined by using HPLC analysis. Morphology of representative adhered MC3T3-E1 cells on b) 13.6-ASO-MIMs and c) 13.6-ASO-NIMs after 24 h of culture at 37 °C, respectively. Morphology of cell adhered d) 13.6-ASO-MIMs and e) 13.6-ASO-NIMs after rinsing with 1.0 M NaCl SPBS. The scale bar corresponds to 200 μm.

further the imprinting effects of our ASO-MIMs. As shown in Figure 5c, the transport fluxes of Ova through the ASO-NIMs were much higher than that of ASO-MIMs. One can reasonably speculate that the imprinting effects produced during the imprinting procedure can form specific recognition sites of Ova on ASO-MIMs surfaces. Furthermore, the permeation factors $\beta_{\text{ASO-NIMs/ASO-MIMs}}$ were all more than 3.5 in the whole permeation experiments, clearly demonstrating the presence of "specific recognition sites" in the ASO-MIMs. As is well-know that the perm-selectivity mechanism of MIMs can be summarized as two diametrically opposite mechanisms (facilitated permeation and retarded permeation).[15] In this work, based on the obtained permeation data of our ASO-MIMs, the second mechanism (retarded permeation) played the main role in the selective separation of Ova protein. The selective separation mechanism is diagrammatically stated in Figure 5d. The template protein Ova could be firstly approached the surface of the ASO-MIMs and then absorbed onto the imprinting cavities. On the contrary, the nontemplate molecules (Lyz, BHb, and Mb in this case) would transport straightforwardly through the channels of the ASO-MIMs with less resistance.

The cell-adhesion behavior of the ASO-MIMs and ASO-NIMs were then investigated in detail by seeding MC3T3-E1 cells (an osteoblastic cell line from normal mouse calvaria) on them. **Figure 6**a showed the adhesion profiles of MC3T3-E1 on ASO-MIMs and ASO-NIMs bound with similar amounts of Ova after 24 h of culture. When the membranes were bound without Ova, the number of adhered cells on the ASO-NIMs was slightly higher than ASO-MIMs, probably because the ASO-MIMs were more hydrophilic (Figure S11, Supporting Information). However, the interesting part was that with the increasing binding amount of Ova molecules, the number of adhered cells on both the ASO-MIMs and ASO-NIMs obviously increased. When the ASO-MIMs were bound with 13.6 mg g^{-1} Ova (13.6-ASO-MIMs), the number of adhered cells was more than four times than that of ASO-MIMs bound without Ova (0-ASO-MIMs), and nearly twice higher than that of 13.6-ASO-NIMs. The obtained obvious increase in cell adhesion ability of ASO-MIMs should be ascribed to the markedly higher association constant of the biocompatible imprinting cavities, which resulted in decreased leakage of Ova from the ASO-MIMs compared to that from the ASO-NIMs (Figure 4, Table 1). One other thing to note is that when bound amount was 19.9 mg g^{-1} or more (more than the apparent maximum number of N_{max}, Table 1), the number of adhered cells dropped gradually. One can reasonably speculate that the redundant Ova competed with surface-bound Ova and weakened the cell adhesion environment. Therefore, when a higher portion of Ova was bound with nonspecific sites, the release of Ova would increase. For the same reason, an almost destructive effect on cell adhesion was obtained because of the more serious leakage and much lower affinity of template protein (Table 1). Nevertheless, it was clear that the Ova-bound 13.6-ASO-MIMs consistently showed better cell adhesion than the 13.6-ASO-NIMs. In addition, cells on the 13.6-ASO-MIMs had better spread morphology after 24 h of culture (Figure 6b,c). Meanwhile, the formative cell sheets on 13.6-ASO-MIMs and 13.6-ASO-NIMs could be successfully detached without hurting the cells after rinsing with 1.0 M NaCl SPBS (Figure 6d,e). The microbiological toxicity experiments were also carried out to further confirm the antibacterial properties of the as-prepared ASO-MIMs. As shown in Figure S12, Supporting Information, the ASO-MIMs exhibited high antibacterial activity against pathogenic bacteria to living cells, and even after 10 cycling operations, the regenerated ASO-MIMs still possessed high antibacterial property, suggesting the excellent structural stability and antibacterial properties of the synthesized ASO-MIMs. In addition, the cell adhesion and detachment behavior of the Ova-bound ASO-MIMs and the ASO-MIMs with covalently immobilized Ova (denoted as ASO-MIMs-C) were compared. As shown in Figure S13, Supporting Information, although the cell adhesion efficiency on the noncovalently bound 13.6-ASO-MIMs was nearly the same with the ASO-MIMs-C, the cell detachment rate from the ASO-MIMs was much higher than that of the ASO-MIMs-C. Taken together, these results clearly demonstrated that the "specific binding" on MIPs can be used as a more efficient approach to immobilizing Ova to promote cell adhesion. And a cell detachment phenomenon could be obtained after the release of Ova molecules through a simple washing process.

The biocompatibility was also investigated to further confirm the cell adhesion performance of our ASO-MIMs. Utilizing the biocompatibility of the ASO-MIMs bound with different amount of Ova, we carried out the bioimaging test by confocal fluorescence microscopy, and the cell-attached samples were rinsed by SPBS and stained by fluorescein diacetate (FDA). The bare glass was used as control system. When comparing **Figure 7**a,b, the relative in vitro viability tests (Figure 7h) and morphological observations showed no significant difference between bare glass and 13.6-ASO-MIMs, indicating the good biocompatibility of 13.6-ASO-MIMs. Meanwhile, as shown in

© 2015 WILEY-VCH Verlag GmbH & Co. KGaA, Weinheim

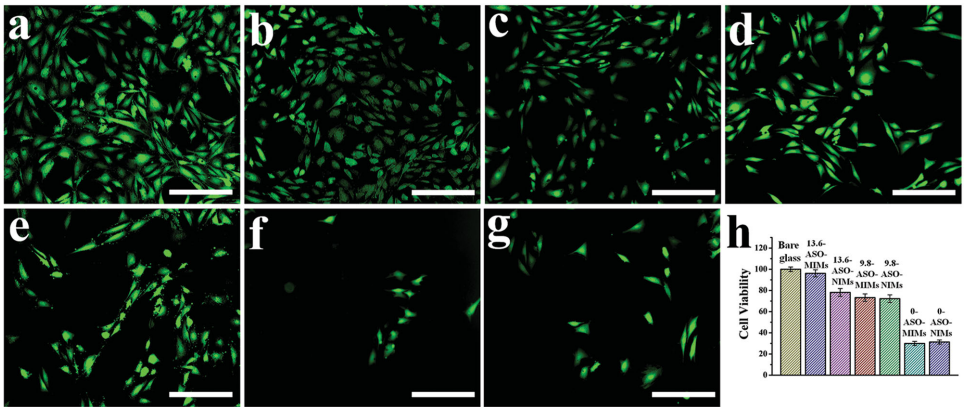

Figure 7. In vitro biocompatibility of the ASO-MIMs and ASO-NIMs bound with different amount of Ova. Confocal fluorescence image the MC3T3-E1 cells incubated with a) bare glass, b) 13.6-ASO-MIMs, c) 13.6-ASO-NIMs, d) 9.8-ASO-MIMs, e) 9.8-ASO-NIMs, f) 0-ASO-MIMs, and g) 0-ASO-NIMs. h) Viability of MC3T3-E1 cells after 48 h of incubation with different membranes. For ease of comparison, each result on the control (bare glass) was designated as 100% scale. The scale bar corresponds to 200 μm.

Figure 7c–e, the relative less attached cells could be found on surfaces of 13.6-ASO-NIMs, 9.8-ASO-MIMs, 9.8-ASO-NIMs. It is worth noting that relative strong fluorescence intensity could be observed from 9.8-ASO-MIMs compared with 9.8-ASO-NIMs, which was agreed with the cell-adhesion experiments (Figure 6). In contrast, from Figure 7f,g, one can clearly see that the relative in vitro viability tests and morphological observations showed no significant difference and considerably fewer attached cells were found on both 0-ASO-MIMs and 0-ASO-NIMs. In addition, morphologies of the MC3T3-E1 cells on pristine RC substrate and other synthesized membranes were also studied as control (Figure S14, Supporting Information). The biocompatibility of the ASO-MIMs bound with different amount of Ova was evaluated by the viability of MC3T3-E1 cells after incubation with the membranes for 24 h by a 3-(4, 5 dimethyl-thiazoyl-2)-2,5 diphenyl tetrazolium bromide (MTT) assay, ASO-NIMs were used as the control system (Figure 7h). As shown in Figure 6h, the cell viability of MC3T3-E1 on 13.6-ASO-MIMs showed no apparent loss, indicating the excellent biocompatibility and nontoxicity of the 13.6-ASO-MIMs. When the amount of the bound Ova was reducing, the ASO-MIMs and ASO-NIMs exhibited reduced cell viability. The 0-ASO-MIMs and 0-ASO-NIMs showed less than 30% of the cell viability (Figure 7h). Collectively, the Ova-bound ASO-MIMs could be demonstrated as a versatile membrane with improved durability, regeneration ability, and biocompatibility.

3. Conclusion

In summary, we have, for the first time, proposed a methodology involving straightforward synthesis techniques for preparing Ag/SiO_2/organic based protein-imprinted membrane, which was innovatively used as a highly efficient novel system for harvesting controllable cell culture substrate and selectively separation of specific bioprotein. The multiple-functional sandwich structure was created by evaluating a two-step functionalization approach onto the mussel-inspired reaction platform (strong covalent surface), thus facilitating the uniform and high-stability growth of Ova-imprinted polymer layers. Importantly, our results showed that the adsorption capacity, selective separation performance, regeneration ability, antibacterial properties and structural stability of the synthesized ASO-MIMs were all remarkably improved. More importantly, in comparison with the covalent immobilization approach, the specific binding in the ASO-MIMs proved to not only promote cell adhesion during cell culture, but also facilitate cell detachment through a simple elution process (the formative confluent cell monolayer could be easily detached by rinsing with 1.0 M NaCl SPBS without hurting the cells and their ECM). We also noticed that, the 13.6-ASO-MIMs exhibited nearly the same biocompatibility and cell-adhesion behavior with bare glass. Meanwhile, the cell viability of 13.6-ASO-MIMs was considerably higher than that of 13.6-ASO-NIMs. These meaningful discoveries can be explained by the formation of the reversible "specific biocompatible recognition sites" toward Ova on ASO-MIMs surfaces. Finally, we envision that this study opens a new direction to biofunctionalization of MIMs and provides a simple yet convenient way to obtain controllable cell culture substrate, which will be ideally suited for bioseparation and cell-based medicine and applications.

4. Experimental Section

Modifying RC by Self-Polymerization Composite of Dopamine Followed by the Hydrolysis of TEOS: Initially, in a typical bionic pDA modification experiment, dopamine (2 mg mL^{-1}) was dissolved in tris(hydroxymethyl) aminomethane (Tris-HCl, 10×10^{-3} M, pH 8.5, Aldrich), the RC substrates were then dipped into the solution under persistently mechanically stirred at room temperature for different time periods, and the pH-induced oxidation changes the solution color to dark brown.[26] The pDA@RC substrates were obtained after rinsing with ultrapure water and dried by N_2 gas. Next, one piece of the as-obtained pDA@RC was dipped into a mixture containing TEOS (2.5 mL, Aldrich), water (12 mL), and ethanol (31 mL) for 60 min, the mixture was incubated with shaking for 1 h. Then, NH_4OH (4.5 mL) was added to the above solution, and the reaction was performed for 3 h. After washing by ethanol and water, the as-prepared SiO_2 modified surfaces (SiO_2@pDA@RC) were desiccated by vacuum at room temperature.

Functionalizing SiO_2@pDA@RC by Acid-Directed Assembly of Ag Nanosheets Followed by the Modification of MPTS: The obtained SiO_2@

© 2015 WILEY-VCH Verlag GmbH & Co. KGaA, Weinheim

pDA@RC were doped in citric acid (CA, 0.25 M) aqueous solution for 2 d, the doped membrane was then rinsed with water to remove the surface adsorbed CA. The doped SiO_2@pDA@RC were first immersed in silver nitrate ($AgNO_3$, 0.1 M, Aldrich) aqueous solution for 1 min, and the CA aqueous solution (10 mL, 0.25 M) was then added to the above solution to direct the assembly of Ag nanosheets on membrane surfaces. The Ag-based surfaces (Ag-SiO_2@pDA@RC) were then carefully rinsed with deionized water to terminate the reaction and desiccated by vacuum at room temperature. The obtained Ag-SiO_2@pDA@RC was then modified with MPTS to introduce the polymerizable double bond for further redox-initiated imprinting procedure. Briefly, Ag-SiO_2@pDA@RC (one piece) and MPTS (2.0 mL) were dispersed in ethanol-water (4:1, v/v) solution (60 mL). The result mixture was heated at 80 °C for 24 h under magnetic stirring (80 rpm). Finally, the obtained functional products (MPTS-Ag-SiO_2@pDA@RC) were washed with ethanol for several times and dried to constant weight.

Synthesis of Ag/SiO_2/Organic Based Hybrid MIMs: The prepolymerization system, composed of AAm (72 mg) and *N*-[3-(dimethylamino) propyl] methacrylamide (DMAPMa, 72 µL, Aldrich) as the monomers, Ova (15 mg) as the template protein and MBAA (155 mg) as the cross-linker, were dissolved in SPBS (pH = 7.2, 0.01 M, 20 mL). After filtered with a 0.22 µm membrane, the solution was firstly purged with N_2 for 15 min. Then one piece of the as-obtained MPTS-Ag-SiO_2@pDA@RC was dipped in the prepolymerization system, followed by the addition of ammonium persulfate (APS, 5 mg, Aldrich) and *N,N,N′,N′*-tetramethylethylenediamine (TEMED, 5 µL, Aldrich). The redox-initiated polymerization were then initiated and lasted for 12 h at 37 °C. After polymerization, the resultant Ag/SiO_2/organic based hybrid MIMs (denoted as ASO-MIMs) was alternately washed with ultrapure water and 1.0 M NaCl SPBS for several times to remove the unreacted monomers and the template protein. The nonimprinted membranes (ASO-NIMs) were prepared by the same procedure but without Ova addition.

Binding and Permeation Assays: For the rebinding experiments, the ASO-MIMs or ASO-NIMs were suspended in Ova SPBS (10 mL, various concentrations) and incubated at 37 °C for different times. After the incubation, the amounts of BHb remaining in the supernatants were determined by high performance liquid chromatography (HPLC). The amount of adsorbed target protein (B) was quantified from the following formula by referring to a calibration curve obtained with a known Ova concentration under the same conditions:

$$B = (C_0 - C_F)V/m \tag{1}$$

where C_0 is the initial Ova concentration, C_F is the equilibrium concentration of Ova remaining in the supernatant, V is the total volume of the binding aliquot, and m is the weight of ASO-MIMs or ASO-NIMs.

In competitive permeation tests, the permeation fluxes of different target proteins for ASO-MIMs and ASO-NIMs were measured by analyzing an aliquot of the SPBS solution from the receiving phase by HPLC method. In addition, to the most precise information for different modules, each experiment was repeated for three times. The permeation flux J (mg cm^{-2} h^{-1}), permeability coefficient P (cm^2 s^{-1}), and perm-selectivity factor β are obtained as follows:

$$J_x = \frac{\Delta C_x V}{\Delta t A} - x = \text{Ova, BHb, Mb, Lyz} \tag{2}$$

$$P = \frac{J_x d}{C_{Fx} - C_{Rx}} - x = \text{Ova, BHbMb, Lyz} \tag{3}$$

$$\beta_{i/j} = \frac{P_i}{P_j} - i, j = \text{Ova BHb, Mb, Lyz, ASO} - \text{MIMs, ASO} - \text{NIMs} \tag{4}$$

where V, A, and d represent the volumes of feeding and receiving SPBS solution (mL), effective membrane area (cm^2), and the membrane thickness, respectively. $\Delta C_x/\Delta t$ is the change of concentration in the receiving solution. (C_{Fx}–C_{Rx}) is the concentration difference between feeding and receiving chambers.

Characterization Techniques: The SEM images were taken on a FEI Sirion-200 scanning electron microscope. The ATR-FTIR for different membranes were recorded on a FT-IR Nicolet560 apparatus (Nicol, U.S.A.), and ZnSe was used as the crystal plate. XPS was recorded using a monochromatized Al Kα X-ray source with an ESCALAB 250 spectrometer. The pressure in the analysis chamber was maintained at 5.0×10^{-8} Torr or lower during each measurement. HPLC containing two LC-20AD Solvent Delivery Units, an SUS-20A gradient controller, and an SPD-20A Detector (Agilent 1200 series, U.S.A.) was used for the determination of BHb, Lyz, Ova, and Mb. The conditions of determination were as follows: mobile phase A was HPLC-grade acetonitrile/H_2O (ACN/H_2O, 80/20, v/v, containing 0.1% trifluoroacetic acid), mobile phase B was ACN/water (90:10, v/v, containing 0.1% trifluoroacetic acid), 1.0 mL min^{-1} flow rate, and the wavelength of UV detector was set at 214 nm.

Cell Culture and Adhesion Study: MC3T3-E1 cells were grown under a humidified atmosphere in α-minimum essential media supplemented with 10% fetal bovine serum (FBS) and 1% penicillin/streptomycin in 5% CO_2 at 37 °C. The medium was changed twice weekly, and the cells were harvested using 0.25% trypsin and EDTA (0.26×10^{-3} M) in SPBS after reaching subconfluency. For cell adhesion, MC3T3-E1 cells were seeded onto the ASO-MIMs or ASO-NIMs (bound with various amount of) Ova at a density of 1×10^4 cells per well, and cultured at 37 °C under a humidified atmosphere of 5% CO_2 for 2 d.[45,46] For cell detachment experiments, the formative cell sheets on the ASO-MIMs surface were then carefully rinsed with 1.0 M NaCl SPBS. Before observation, the cell-attached samples were rinsed by SPBS and stained by FDA. The cell viability was determined using an MTT assay. The MTT solution (5 mL, 5 mg mL^{-1} 1 in SPBS) was added to each well, and the cells were incubated additionally for 3 h at 37 °C. The resulting formazan crystals were dissolved in dimethylsulfoxide, and the absorbance was measured at 595 nm using a Victor 3 microplate reader (Perkin Elmer Inc., Waltham, MA, USA). The morphology of MC3T3-E1 osteoblasts were observed by a confocal laser scanning microscopy (CLSM, Leica DMIRE 2). Cell number per unit area in the photographs was counted and averaged from three separate experiments.

Supporting Information

Supporting Information is available from the Wiley Online Library or from the author.

Acknowledgements

This work was financially supported by the National Natural Science Foundation of China (Nos. 21446015, 21406085, U1407123), Ph.D. Programs Foundation of Ministry of Education of China (No. 20123227120015), Natural Science Foundation of Jiangsu Province (BK20140580), and Special Financial Grant from the China Postdoctoral Science Foundation (2014T70488).

Received: June 16, 2015
Revised: July 29, 2015
Published online: August 13, 2015

[1] N. Huebsch, D. J. Money, *Nature* **2009**, *462*, 426.
[2] R. V. Bellamkonda, *Nat. Mater.* **2008**, *7*, 347.
[3] M. Garta, R. Malpass-Evans, M. Croad, Y. Rogan, J. C. Jansen, P. Bernardo, F. Bazzarelli, N. B. McKeown, *Science* **2013**, *339*, 303.

© 2015 WILEY-VCH Verlag GmbH & Co. KGaA, Weinheim

[4] D. L. Gin, R. D. Noble, *Science* **2011**, *332*, 674.
[5] E. Krieg, H. Weissman, E. Shiman, B. Rybtchinski, *Nat. Nanotechnol.* **2011**, *6*, 141.
[6] Y. Miyahara, N. Nagaya, M. Kataoka, B. Yanagawa, K. Tanaka, H. Hao, K. Ishino, H. Ishida, T. Shimizu, K. Kangawa, S. Sano, T. Okano, S. Kitamura, H. Mori, *Nat. Med.* **2006**, *12*, 459.
[7] H. Takahashi, M. Nakayama, M. Yamato, T. Okano, *Biomacromolecules* **2010**, *11*, 1991.
[8] X. L. Wang, H. Zhu, X. X. Liu, F. Yang, X. R. Yang, *Sci. Rep.* **2013**, *3*, 1463.
[9] Y. L. Colson, M. W. Grinstaff, *Adv. Mater.* **2012**, *24*, 3878.
[10] T. G. Kim, H. Shin, D. W. Lim, *Adv. Funct. Mater.* **2012**, *22*, 2446.
[11] S. J. Li, Y. Ge, S. A. Piletsky, A. P. F. Turner, *Adv. Funct. Mater.* **2011**, *21*, 3344.
[12] G. Wulff, *Chem. Rev.* **2002**, *102*, 1.
[13] C. G. Xie, H. F. Li, S. Q. Li, J. Wu, Z. P. Zhang, *Anal. Chem.* **2010**, *82*, 241.
[14] G. Wulff, J. Liu, *Acc. Chem. Res.* **2012**, *45*, 239.
[15] M. Ulbricht, *J. Chromatogr. B* **2004**, *804*, 113.
[16] J. K. Awino, Y. Zhao, *J. Am. Chem. Soc.* **2013**, *135*, 12552.
[17] R. R. Chen, L. Qin, M. Jia, W. Y. Li, *J. Membr. Sci.* **2010**, *363*, 212.
[18] X. F. Zhang, X. Z. Du, X. Huang, Z. P. Lv, *J. Am. Chem. Soc.* **2013**, *135*, 9248.
[19] J. F. Kim, G. Szekely, I. B. Valtcheva, A. G. Livingston, *Green Chem.* **2014**, *16*, 133.
[20] A. Kros, R. J. M. Nolte, N. A. J. M. Sommerdijk, *Adv. Mater.* **2002**, *14*, 1779.
[21] A. F. Ismail, L. I. B. David, *J. Membr. Sci.* **2001**, *193*, 1.
[22] W. L. Li, J. Y. Walz, *Sci. Rep.* **2014**, *4*, 4418.
[23] T. S. Chung, L. Y. Jiang, Y. Li, S. Kulprathipanja, *Prog. Polym. Sci.* **2007**, *32*, 483.
[24] J. Jiang, L. Zhu, B. Zhu, Y. Xu, *Langmuir* **2011**, *27*, 14180.
[25] Y. Mansourpanah, S. S. Madaeni, A. Rahimpour, A. Farhadian, A. H. Taheri, *J. Membr. Sci.* **2009**, *330*, 297.
[26] H. Lee, S. M. Dellatore, W. M. Miller, P. B. Messersmith, *Science* **2007**, *318*, 426.
[27] H. Lee, Y. Lee, A. R. Statz, J. Rho, T. G. Park, P. B. Messersmith, *Adv. Mater.* **2008**, *20*, 1619.
[28] R. X. Zhang, L. Braeken, P. Luis, X. L. Wang, B. Van der Bruggen, *Membr. Sci.* **2013**, *437*, 179.
[29] Y. L. Wu, X. L. Liu, M. J. Meng, P. Lv, M. Yan, X. Wei, H. J. Li, Y. S. Yan, C. X. Li, *J. Membr. Sci.* **2015**, *490*, 169.
[30] D. Ling, W. Park, Y. I. Park, N. Lee, F. Li, C. Song, S. G. Yang, S. H. Choi, K. Na, T. Hyeon, *Angew. Chem. Int. Ed.* **2011**, *50*, 11360.
[31] Q. Liu, N. Y. Wang, J. Caro, A. S. Huang, *J. Am. Chem. Soc.* **2013**, *135*, 17679.
[32] M. Zhang, X. Zhang, X. He, L. Chen, Y. Zhang, *Nanoscale* **2012**, *4*, 3141.
[33] D. H. Kim, H. J. Lee, J. M. Nam, A. Levchenko, *Adv. Mater.* **2010**, *22*, 4551.
[34] B. A. Zangmeister, T. A. Morris, M. J. Tarlov, *Lanmuir* **2013**, *29*, 8619.
[35] L. Shao, Z. X. Wang, Y. L. Zhang, Z. X. Jiang, Y. Y. Liu, *J. Membr. Sci.* **2014**, *461*, 10.
[36] N. Sahiner, O. Ozay, *Colloids Surf. A* **2011**, *378*, 50.
[37] Y. L. Wu, M. Yan, X. L. Liu, P. Lv, J. Y. Cui, M. J. Meng, J. D. Dai, Y. S. Yan, C. X. Li, *Green Chem.* **2015**, *17*, 3338.
[38] Y. Sueyoshi, C. Fukushima, M. J. Yoshikawa, *Membr. Sci.* **2010**, *357*, 90.
[39] Y. Sueyoshi, A. Utsunomiya, M. Yoshikawa, G. P. Robertson, M. D. Guiver, *J. Membr. Sci.* **2012**, *401*, 89.
[40] Y. L. Wu, M. Yan, Y. S. Yan, X. L. Liu, M. J. Meng, P. Lv, J. M. Pan, P. W. Huo, C. X. Li, *Langmuir* **2014**, *30*, 14789.
[41] H. J. Wang, W. H. Zhou, X. F. Yin, Z. X. Zhuang, H. H. Yang, X. R. Wang, *J. Am. Chem. Soc.* **2006**, *128*, 15954.
[42] Y. S. Ho, G. McKay, *Water Res.* **1999**, *33*, 578.
[43] Y. S. Ho, G. McKay, *Process Biochem.* **1999**, *34*, 451.
[44] I. Langmuir, *J. Am. Chem. Soc.* **1918**, *40*, 1361.
[45] J. Ryu, S. H. Ku, W. H. Lee, C. B. Park, *Adv. Funct. Mater.* **2010**, *20*, 2132.
[46] J. C. Bao, Y. Y. Liang, Z. Xu, L. Si, *Adv. Mater.* **2003**, *15*, 1832.

© 2015 WILEY-VCH Verlag GmbH & Co. KGaA, Weinheim